Macromolecules

pubs.acs.org/Macromolecules Article

Lewis Pair Polymerization of Renewable Indenone to Erythro-Ditactic High-T_g Polymers with an Upcycling Avenue

Ryan W. Clarke, Michael L. McGraw, Ravikumar R. Gowda, and Eugene Y.-X. Chen*

Cite This: *Macromolecules* 2020, 53, 640−648 Read Online

ACCESS | Metrics & More | Article Recommendations | Supporting Information

ABSTRACT: Preparation and storage of biorenewable, monomeric indenone, much less the polymerization to a well-defined, high-molecular-weight polymer, is challenging because of anti-aromaticity-driven radical autopolymerization. Herein, we report the successful preparation and subsequent Lewis pair polymerization (LPP) of indenone without autopolymerization side reactions using Lewis pairs consisting of sterically encumbered Lewis acid (LA) catalysts, such as $B(C_6F_5)_3$ and bis(2,6-*tert*-butyl-4-methylphenoxy)methylaluminum and Lewis base initiators such as silyl ketene acetal and N-heterocyclic olefin nucleophiles. Thus, for the first time, the LPP enabled the synthesis of polyindenone (Pin) with high number-average molecular weight (M_n = 1.72 × 10^5 g mol^{-1}) and low dispersity ($Đ$ = 1.13). Observed correlations between the steric bulk of the LA catalyst and diastereoselectivity (57−75%) created the opportunity to model and investigate the relationships between β-substituted monomer motifs, catalyst steric accessibility, and the propagation stereodefining step for ensuing ditactic assignments. Through the increased erythro-diastereoselectivity, semicrystalline materials were produced with remarkably high glass-transition temperatures (T_g = 307 °C), high thermal stability ($T_{d,5\%}$ = 356 °C), and competitive transmittance (T %) and haziness values (T % = 85−88%, haze = 11%). Controlled pyrolysis of Pin upconverted it into versatile graphite oxide with 54% conversion, offering an upcycling avenue for Pin at the end of its life.

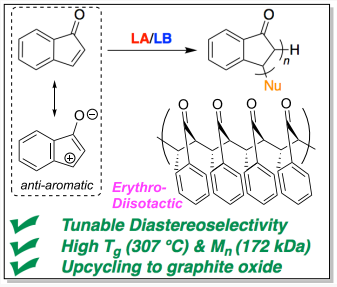

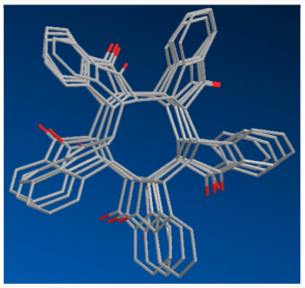

INTRODUCTION

The conjugate-addition polymerization of β-substituted Michael acceptors, which have historically been problematic monomers to polymerize effectively due to their resistance to conventional radical and ionic polymerization methodologies, has been recently reinvestigated using more modern polymerization methods.[1−6] The challenges associated with such monomers are both thermodynamic and chemoselective in nature, making them good candidates to showcase new polymerization methodologies. These β-substituted monomers add new complexity to the existing field of stereoselective polymerization by including two stereogenic centers at each repeat unit, thus requiring additional control for stereoselectivity to produce ditactic polymers. Overall, our interest in β-substituted monomers is twofold: ditactic polymers, while much less explored, could offer intriguing or advanced material properties, and β-substitution is a common motif among many naturally occurring, bioderived Michael acceptors, such as crotonates, sorbates, and cinnamates.[7−12]

A preference in linear β-substituted monomers for disyndiotactic outcomes was generally recognized through a chain-end control mechanism.[13−19] Chain-end selectivity is derived from chirality at the penultimate repeat unit of the growing polymer chain end. In the two most recently studied examples, methyl crotonate and methyl cinnamate, disyndio-rich polymers were obtained based on chiral influence of the methyl and phenyl groups, respectively.[3,20] Following this logic, we hypothesized that a cyclic β-substituted Michael acceptor might exert increased chain-end selectivity because of increased steric hindrance and fewer overall degrees of freedom, thus, fewer possible competing transition states (TSs), subsequently bringing about enhanced chain-end control diastereoselectivity.

While considering a number of endocyclic Michael acceptors to test our hypothesis, we found an unlikely candidate, indenone (**M1**). A simple analysis of this monomer revealed several intriguing properties, first and foremost being the antiaromatic resonance structure produced by classical carbonyl activation (Scheme 1). We reasoned that the additional instability of **M1** due to antiaromaticity could be used as a driving force for polymerization, as antiaromatic compounds are known to rearrange/isomerize to relieve instability by achieving an aromatic or nonaromatic structure.[21,22] Likewise, we recognized that conjugate-addition polymerization of **M1** would relieve antiaromaticity which can thus be used as a driving force, similar to how ring-strain is exploited in ring-

Received: October 31, 2019
Revised: December 14, 2019
Published: January 16, 2020

https://dx.doi.org/10.1021/acs.macromol.9b02285
Macromolecules 2020, 53, 640−648

Scheme 1. Resonance Structure Displaying the Antiaromatic Nature of M1 (2n π-Electrons)

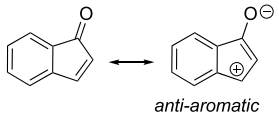

opening polymerization of lactones.[23−26] Indeed, literature examples of **M1** synthesis consistently remarked on the instability of this compound and its predisposition to undergo autopolymerization.[27] In fact, Chandross and Hartless included the statement that "because of its instability, it is not possible to prepare and store indenone" among reported radical copolymerization endeavors.[28]

We also found this monomer intriguing because a recent publication on the cationic polymerization of benzofuran, similar in structure to **M1**, revealed especially high glass-transition temperatures (T_g = 210 °C), presumably because of the fused benzene moiety present within that structure.[29] While considering that incorporation of ketones within polymers often increases the T_g, we hypothesized that polyindenone (Pin) would have a T_g higher than that of poly(benzofuran), perhaps upward of 300 °C, making it useful as an engineering plastic. Last, we recognized the reported syntheses of the precursor 1-indanone from bioderived cinnamic acid with heterogeneous catalysts, which serves as an important characteristic of any renewable polymer in order to reduce both CO_2 emissions and dependency on finite petroleum resources (Scheme S1).[30−33]

Thus, we set out to find appropriate conditions to store indenone and inhibit autopolymerization. Once this task was completed, we sought conditions that would yield a successful and controlled polymerization process by Lewis acid (LA) and Lewis base (LB) pairs, namely, Lewis pair polymerization (LPP), by utilizing synergy and cooperativity of the LA and LB sites.[34−39] To tame the inherent high reactivity of indenone, we chose LA-mediated group transfer polymerization (LA-GTP), as the silyl enolate LB should render a low energy propagating species compared to that of anionic or radical analogues. Moreover, monomer coordination to an LA would generate a highly reactive antiaromatic monomer, allowing us to exploit this characteristic as a driving force for polymerization to achieve high degrees of polymerization, shorter reaction times, and lower catalyst loadings. Following the same logic, we also explored the frustrated Lewis pair (FLP) strategy using bulky LA bis(2,6-*tert*-butyl-4-methylphenoxy)-methylaluminum (MAD) and bulky N-heterocyclic olefin (NHO) 1,3-dimethyl-4,5-diphenyl-2-(propan-2-ylidene)-2,3-dihydro-1*H*-imidazole as the LB, as such an FLP has been shown to bring out living polymerization of polar conjugated alkenes.[40−43] Comparatively, the FLP system should exhibit higher activity than the LA-GTP system because frustrated LPP (FLPP) proceeds through a persistent zwitterionic active species that does not return to a neutral resting state as in LA-GTP. While the persistent zwitterion in FLPP is less stable than the silyl-capped enolate present in LA-GTP, there are no obvious termination or transfer pathways foreseeable for indenone that would give a reason to protect the growing chain. Accordingly, this report presents a full account of our study on the LPP of **M1** by the above described Lewis pairs, including the polymerization characteristics, effects of LA sterics on diastereoselectivity, as well as the properties and an end-of-life option (upcycling avenue) of the resulting polymer.

RESULTS AND DISCUSSION

Indenone Preparation, Storage, and Autopolymerization Control. As mentioned above, **M1** readily undergoes autopolymerization to generate an atactic, amorphous Pin (Figure S2). Accordingly, we developed an effective preparation and storage method involving timely **M1** synthesis from indanone (see the Supporting Information), dilution to a 0.77 M stock solution in dichloromethane (DCM), and storage at −30 °C, which enabled elimination of autopolymer contaminants in catalyzed samples and longer-term access to monomeric indenone for polymerization studies (Figure S4). To investigate the effectiveness of our indenone storage method over a 7-day period, aliquots were taken every 24 h from the mother stock solution and analyzed by ^{1}H NMR. In each experiment, there were no signals for the methine protons characteristic of polymer formation between 2.0 and 4.0 ppm (Figure S5). As a control to test autopolymerization of **M1** under the storage concentration, a sample of the monomer solution was stirred (without additives) in a dark, room-temperature (RT, ∼23 °C) environment within an inert atmosphere. After stirring under such conditions for 24 h, no Pin signals were observed by ^{1}H NMR (Figure 1), indicating

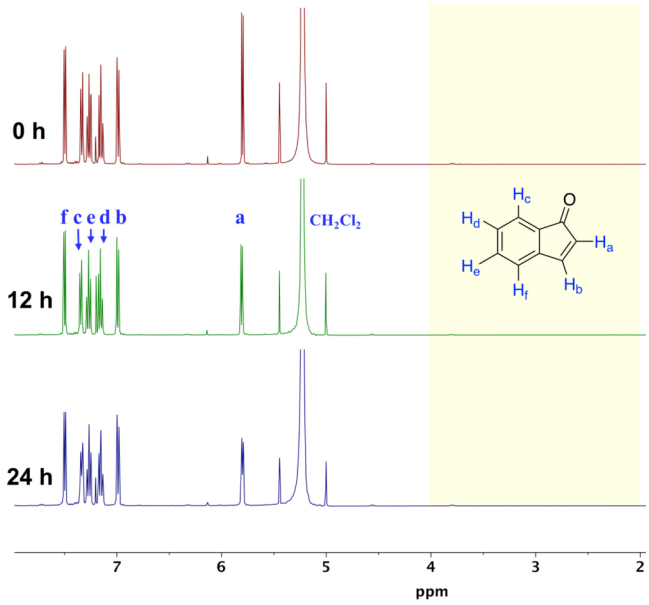

Figure 1. Overlay of ^{1}H NMR spectra ($CDCl_3$) of reaction aliquots of additive-free stirring of **M1** stock solution (0.77 M in DCM) under dark, RT, and inert atmosphere conditions as a function of time, 0 h (top), 12 h (middle), and 24 h (bottom), indicating that **M1** is stabilized against autopolymerization side reactions under such conditions.

that **M1** is stable under dilute, dark conditions, thereby allowing sufficient time to execute LPP experiments without autopolymerization interference. On the other hand, stirring bulk indenone under ambient conditions led to gelation, and this autopolymerized sample as a firm gel was collected after 72 h and analyzed by ^{13}C NMR (Figure S6) and gel permeation chromatography (GPC) to serve as a comparison to catalyzed Pin samples described below.

https://dx.doi.org/10.1021/acs.macromol.9b02285
Macromolecules 2020, 53, 640−648

Scheme 2. Outlined Initiation and Propagation Mechanisms for the LPP of M1 by LA/SKA LP via the Established LA-GTP (Left) and by FLP LA/NHO via the Established Zwitterionic LPP (Right)

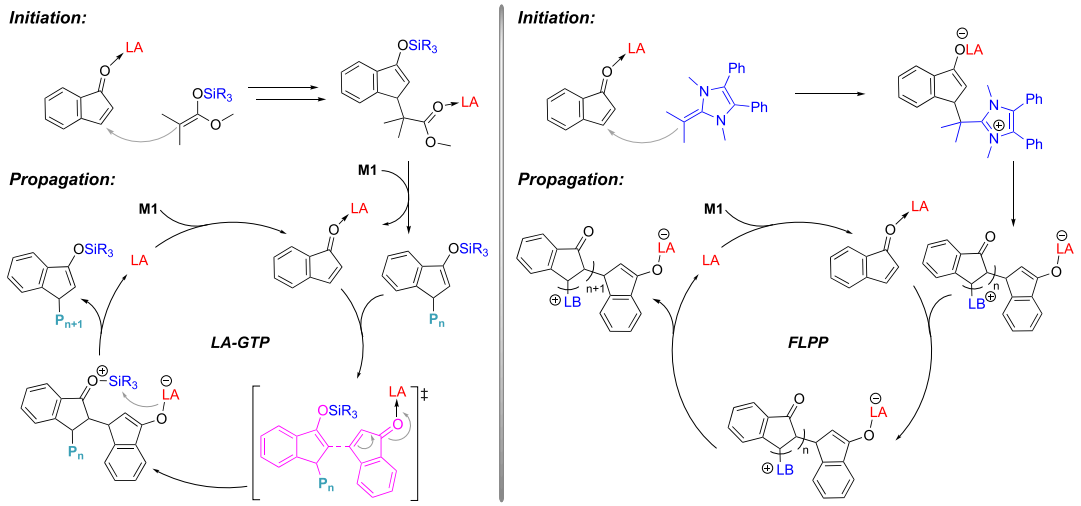

Table 1. Selected Results for LPP of M1[a]

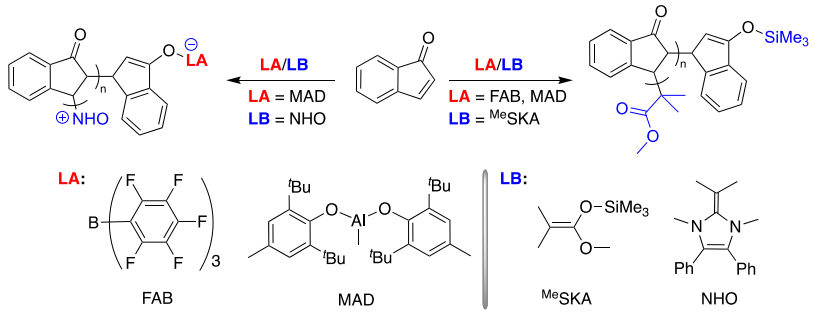

run[a]	LA	LB	M1/LA/LB	time (h)	isolated yield (%)	M_n[b] (kg/mol)	$Đ$[b] (M_w/M_n)	T_g[c] (°C)
1	n/a	n/a	n/a	72	87	205	1.91	269
2	FAB	^{Me}SKA	300:2:1	12	99	81	1.13	271
3	FAB	^{Me}SKA	500:2:1	12	99	172	1.23	286
4	MAD	^{Me}SKA	500:2:1	12	99	[d]	[d]	292
5	MAD	^{Me}SKA	1000:2:1	24	99	[d]	[d]	307
6	MAD	NHO	500:2:1	1	99	[d]	[d]	303
7	MAD	NHO	1000:2:1	2	99	[d]	[d]	n/d

[a]Polymerization conditions: [**M1**] = 0.77 M (DCM) for runs 2−7; [**M1**] = bulk for run 1, where run 1 represents autopolymerization beyond gelation without initiator/catalyst additives. Runs 2−7 were performed in dark at RT in an Ar-filled glovebox. NHO was prepared in a toluene stock solution as it slowly decomposes in DCM prior to initiation. n/a = not applicable; n/d = not determined. [b]M_n and $Đ$ values determined by GPC at 40 °C in $CHCl_3$ coupled with a DAWN HELEOS II multi(18)-angle light scattering detector and an Optilab TrEX dRI detector for absolute M_w. [c]Determined by differential scanning calorimetry. Values were obtained from the second heating scan with a heating rate of 15 °C/min. [d]Not measured due to stereoselectivity-induced insolubility in common GPC solvents ($CHCl_3$, THF, and DMF).

Polymerization Results and Key Characteristics. With an autopolymerization-free preparation and a storage method established, **M1** was investigated for controlled polymerization to a possibly high molecular weight (M_w), functionalized ditactic polymer. Considering the Michael acceptor motif and the highly reactive propagating enolate, we hypothesized that LA-GTP would tame the reactivity of the actively growing chain enolate and inhibit chain-transfer pathways to facilitate a slower, more controlled propagation (Scheme 2). We began by testing this LA-GTP with sterically encumbered LA $B(C_6F_5)_3$ (FAB) paired with LB/initiator dimethylketene methyl trimethylsilyl acetal (^{Me}SKA), which have been employed to execute GTP on a wide range of Michael acceptor-type monomers.[44−46] It should be noted here that background polymerization activity was not observed by either FAB or ^{Me}SKA, individually, with [**M1**]/[FAB] or [**M1**]/[^{Me}SKA] = 100/1 at RT for 24 h.

The polymerization reactions were carried out under dark and RT conditions using FAB and ^{Me}SKA in a 2:1 ratio with catalyst/initiator loadings between 0.1 and 0.6 mol % relative to **M1**. Each reaction was quenched at either 12 or 24 h, achieving quantitative (>99%) isolated yields. Isolated polymer samples had M_n values between 8.1×10^4 and 1.72×10^5 g mol^{-1} and dispersity $Đ$ values between 1.13 and 1.23 (Table 1, run 2−3). The low dispersity $Đ$ values, coupled with a monomodal M_w distribution (Figures S7), indicate the absence of parallel autopolymerization, which was verified by our control experiments (vide supra). A low M_w Pin sample with a

https://dx.doi.org/10.1021/acs.macromol.9b02285
Macromolecules 2020, 53, 640−648

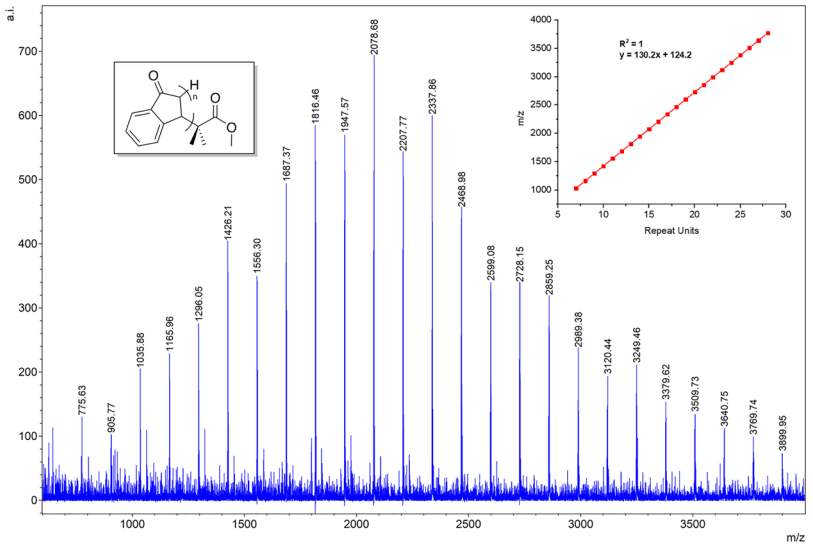

Figure 2. MALDI-TOF MS spectrum for a low M_w Pin sample prepared by [**M1**]/[FAB]/[^{Me}SKA] = 20/2/1 and end-group analysis supporting initiation by the proper ^{Me}SKA LB.

theoretical M_n of 2.60 × 10^3 g mol^{-1} was further analyzed by matrix-assisted laser desorption/ionization time-of-flight mass spectroscopy (MALDI-TOF MS). A near-ideal bell-curve was observed with the absence of competing peaks related to possible autopolymerization pathways (Figure 2). End-group analysis revealed a mass of 124.2 g mol^{-1}, which correlates to $-Me_2CO_2Me$ (from initiation by the initiator ^{Me}SKA), a proton (from acidic quenching), and a sodium cation (used to ionize the polymer).

Guided by the hypothesis for LA-mediated chain-end control (c.f. Scheme 2), we further examined the effect of the LA on this LPP by employing a more sterically hindered LA, MAD, which alone did not promote any polymerization (1.0 mol %, RT, 24 h). Polymerizations with [**M1**]/[MAD]/[^{Me}SKA] = 500/2/1 (run 4) and 1000/2/1 (run 5) afforded Pin materials that are insoluble in common organic solvents ($CHCl_3$, DCM, THF, toluene, etc.,), precluding GPC analysis for M_w information. In fact, the only solvent that would solubilize the MAD-catalyzed Pin was trifluoroacetic acid (TFA) because of enhanced erythro selectivity (71%, vide infra). Switching the LB to NHO, the polymerization by the MAD/NHO LP was much faster, achieving quantitative isolated polymer yield in 1 h or 2 h for the run with [**M1**]/[MAD]/[NHO] = 500/2/1 (run 6) and 1000/2/1 (run 7). The sterically demanding and acidic-proton-lacking NHO with α,α-dimethyl substitution was chosen in particular (apart from other NHOs, NHCs, and conventional LBs) because it forms a truly FLP with MAD, and its structure lends itself to predictable reactivity as a potent nucleophile, unlikely to participate in any termination/transfer reactions. Unlike LA-GTP, the NHO/MAD pair facilitates a typical LPP mechanism, where the propagating chain would have a cationic initiation end-group and forces the polymerization to proceed through a zwitterionic intermediate (Scheme 2, right column). Thus, this zwitterionic LPP exhibits enhanced activity compared to the LA-GTP mechanism, which is able to escape the zwitterionic intermediate through the silylium recapture (Scheme 2, left column). On the other hand, this MAD-catalyzed LPP also afforded Pin with the same insolubility in common organic solvents, characteristic of high erythro-selectivity (75%, vide infra). Although this insolubility precludes GPC analysis, the possibility of high-M_w-induced insolubility was ruled out by MALDI-TOF MS analysis of insoluble Pin oligomers produced by the FLP MAD/NHO. The MALDI spectrum highlights a near-ideal bell curve, while end-group analysis revealed the NHO as the initiator (Figure S8).

Polymerization Stereoselectivity and Polymer Ditacticity Assignments. The stereoregularity of Pin materials synthesized by LPP using different LPs was ascertained by quantitative ^{13}C NMR analysis in TFA-d_1 for solubility reasons. As the carbonyl signal (δ = 208.5 ppm) is the most sensitive to the stereoenvironment, it was chosen for comparison of different Pin materials (Figure 3). The full ^{13}C NMR spectrum of Pin along with peak assignments can be found in Figure S3. As compared to the atactic, amorphous Pin by autopolymerization, the Pin by FAB/^{Me}SKA LP showed notable intensity enhancement in the resonance at 208.5 ppm, relative to two

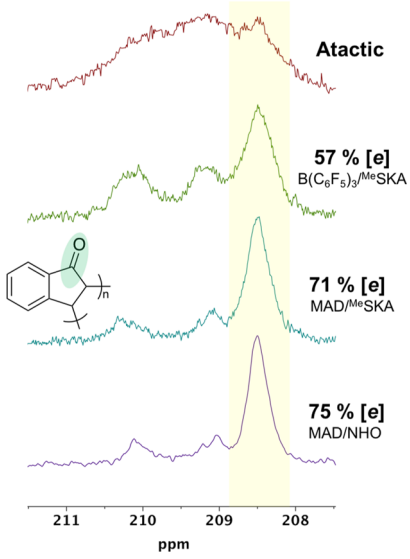

Figure 3. Expanded carbonyl region of ^{13}C NMR (125 MHz, TFA-d_1) spectra of Pin materials produced by autopolymerization and LPP with different LPs as labeled. [e] = erythro-di(*iso*)tactic.

https://dx.doi.org/10.1021/acs.macromol.9b02285
Macromolecules 2020, 53, 640−648

Scheme 3. Predicted TSs Promoting Erythro-Diastereoselective Propagation (Left) vs Disfavored Threo-diastereoselective Propagation (Right) during LA-Mediated GTP[a]

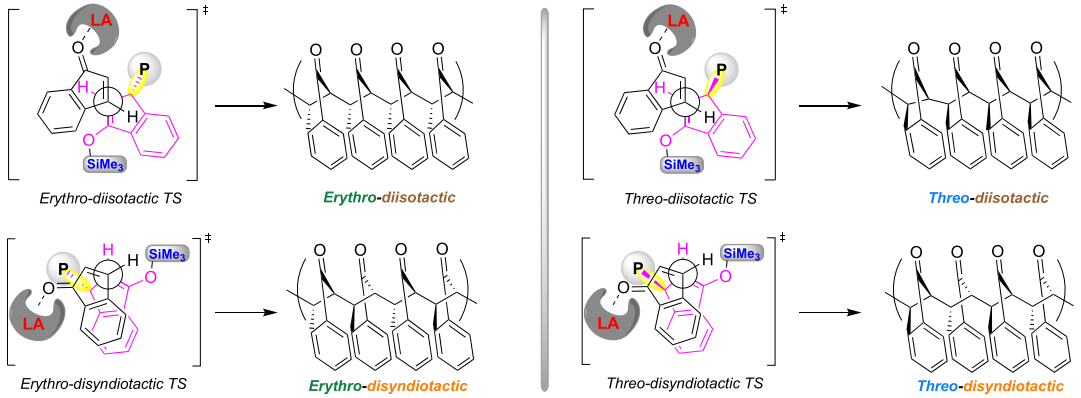

[a]Accompanied are visuals of the four possible stereochemical arrangements for a ditactic Pin.

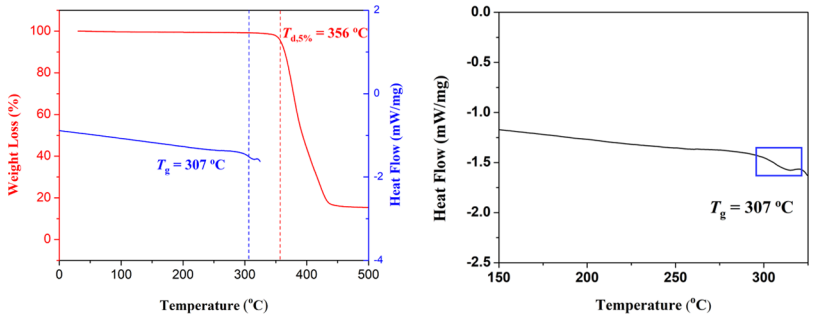

Figure 4. Left: an overlay of TGA (red curve) and DSC (blue curve) traces for 71% erythro-ditactic Pin with labeled $T_{d,5\%}$ and T_g values, highlighting that the endotherm (T_g) on the DSC trace is not due to decomposition. Right: separate DSC curve of the same sample.

other peaks centered at ~209 and ~210 ppm in the carbonyl region (Figure 3), revealing enhanced stereoregularity (to 57%). As a new homopolymer without prior reported tacticity assignments by ^{13}C NMR, Newman projections of the staggered propagation TSs were modeled to compare the stereodefining step. Pin has two stereocenters on each repeat unit and is thus ditactic, where threo-diisotactic, erythro-diisotactic, threo-disyndiotactic, or erythro-disyndiotactic arrangements on the polymer backbone are possible. As the LA-activated **M1** species encounters a growing chain, we postulate that the TS will favor an interaction in which the sterically encumbered LA-activated monomer and the large silyl group will oppose each other spatially to suppress steric interactions (Scheme 3).

Of the four possible Newman projections, two (related to threo-diastereoselective outcomes) seem unreasonable because they involve the penultimate polymer repeat unit (and the rest of the chain) pointed in the direction of the incoming monomer. The other two Newman projections, involving the polymer chain pointed back and away from the TS (highlighted in yellow), are related to erythro-diisotactic and erythro-disyndiotactic units and seem the most reasonable (Scheme 3). Although we will not speculate on which erythro projection is most favorable, we will point out that erythro-diisotactic is more consistent with thermal analysis and powder X-ray diffraction (pXRD) data as well as solubility observations, discussed below. However, distinguishing between the two possible erythro structures requires further evidence.

Figure 3 revealed a large LA effect on the erythro-ditacticity of the resulting Pin. When switching the LA paired with ^{Me}SKA from FAB to MAD, the selectivity was enhanced from 57 to 71%. Most intriguingly, the Pin with 71% stereoregularity or higher becomes insoluble in common organic solvents tested (vide supra), consistent with the increased stereoregularity and/or crystallinity of the polymer. The highest erythro-diastereoselectivity (75%) in this series was produced by the MAD/NHO LP, revealing less influence by the LB on the selectivity of the resulting Pin. The steric effects of the LA on diastereoselectivity can be ascribed to its influence on the stereochemical defining TSs (whether erythro-diisotactic or -disyndiotactic defining). Referring to the reasoned Newman projections (Scheme 3), the more sterically encumbered MAD should widen the energy gap between the two competing propagating TSs and thus suppress stereoerrors. In the case of the zwitterionic LPP by the MAD/NHO FLP, the two sterically encumbered LA equivalents are responsible for both activating the free monomer and protecting the active enolate chain end. Thus, the ditacticity is enhanced through additional LA steric influence (Scheme 2) because of the further increased energy gap between the competing TSs and suppressed stereoerror. We attempted to further increase the diastereoselectivity by using sterically more demanding LAs including $EtAl(BHT)_2$ and $^{i}BuAl(BHT)_2$. However, no noticeable improvement in selectivity was realized by NHO/$EtAl(BHT)_2$, while no polymerization activity was observed with NHO/$^{i}BuAl(BHT)_2$. Therefore, new and more effective catalyst design would be necessary to achieve greater diastereoselectivity. The spectra in Figure 3 (with the exception of the atactic Pin) have one large peak accompanied by two smaller peaks. Interestingly, the two minor peaks always

https://dx.doi.org/10.1021/acs.macromol.9b02285
Macromolecules 2020, 53, 640−648

share similar integration. Therefore, we hypothesize that the major peak represents the erythro-diastereoselective units, while the two minor peaks represent carbonyls at the interface of an erythro-diisotactic/disyndiotactic stereoerror (Figure S9).

Erythro-Ditactic Pin Material Properties. Thermal properties of Pin materials with varied erythro-ditactic contents were examined by thermal gravimetric analysis (TGA) and differential scanning calorimetry (DSC). All the Pin materials produced by LPs showed nearly identical $T_{d,5\%}$ (decomposition temperature defined by the temperature at 5% weight loss) values between 354 and 356 °C (Figure 4), while the autopolymerized Pin exhibited noticeably lower thermal stability with a T_d of 329 °C (Figure S10). The overall increased thermal stability for the Pin produced by LPs is presumably due to the enhanced regioselectivity and stereoselectivity through the controlled polymerization via the LPP mechanisms. This reasoning was further supported by the observation that the autopolymerized Pin exhibited a visible shouldering and a multistep decomposition profile (Figure S10), attributable to differences in its head/tail, head/head, and tail/tail linked units (regio-irregularities) by the non-selective radical polymerization process.

DSC traces of the LP-produced Pin showed uniquely high T_g values but no obvious melting-transition temperature (T_m) or crystallization temperature. For example, the Pin produced by the MAD/NHO LP with 71% stereoregularity had an exceptionally high T_g of 307 °C (Figure 4). The T_g values of other Pin samples with varied M_w and diastereoselectivity were in the range of 271 and 303 °C (Figures S12−S17), comparable to that of the autopolymerized Pin (269 °C, Figure S11). Noted, the Pin sample with the highest diastereoselectivity (75%) of the series, coupled with a high theoretical M_w of $M_n = 6.50 \times 10^5$ g mol^{-1} displayed no clear T_g, suggesting that it may be near or above the decomposition temperature ($T_{d,5\%}$ = 356 °C). For the same possible reason, no T_m, which in theory should be much above the T_g, was observed for all Pin samples.

To explain the insolubility of the Pin when the erythro-ditacticity reaches about 70%, we hypothesized that at some erythro-ditactic content threshold, Pin may assemble into a secondary structure that increases overall crystallinity and chain rigidity. We probed this hypothesis by modeling a 20-mer of erythro-diisotactic and erythro-disyndiotactic Pin using molecular mechanics 2 (MM2, see the Supporting Information), which in the case of the former, rearranged to predict a 5_1 helical secondary structure (Figure 5). Erythro-disyndiotactic conditions led to a random coil architecture. It should be noted here that this computational result solely shows the plausibility of helical secondary structures and does not rule out erythro-disyndiotacticity. However, although this does not provide full support for either assignment in our specific sample, it does leads us to surmise that if secondary structures such as helices are produced, an increase in crystallinity and diminished solubility in common organic solvents due to the presence of well-ordered structures would be observed.

To seek additional evidence for erythro-diisotacticity-induced crystallinity, we performed pXRD analysis on the Pin with 75% erythro-ditacticity in parallel to the atactic, amorphous autopolymerized Pin. The atactic, amorphous Pin showed only two broad signals at 9.8 and 21.9°, corresponding to d spacings of 0.90 and 0.41 nm, respectively (Figure 6). In contrast, the pXRD patterns of the erythro-ditactic Pin feature

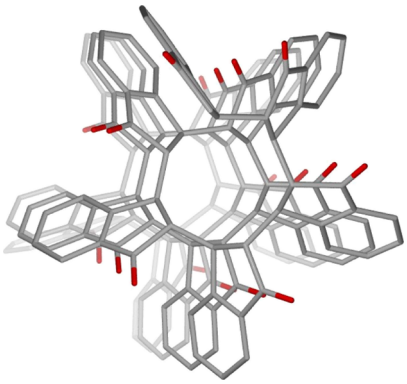

Figure 5. Predicted 5_1 helical secondary structure for erythro-diisotactic Pin by MM2 calculations.

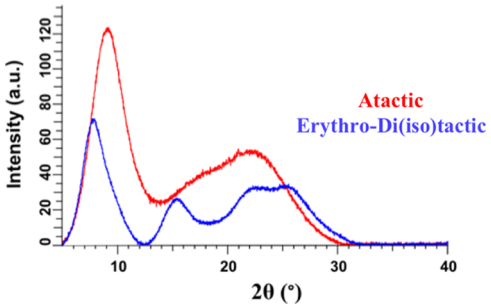

Figure 6. pXRD plots of autopolymerized Pin (red) and LP-induced Pin with 75% erythro-ditacticity (blue) between 5 and 40°.

four resolved, much sharper diffraction peaks at 7.3, 15.2, 22.5 and 25.3°, corresponding to d spacings of 1.2, 0.58, 0.39, and 0.35 nm, respectively, which is consistent with the enhanced crystallinity for the diastereoselective Pin. Through pXRD and MM2 models, it is more likely that the TS stereo-defining step produces erythro-diisotactic, helical Pin reflecting heightened crystallinity and suppressed solubility. Collectively, our findings from the analyses of solubility, Newman projections, NMR-derived diastereoselectivity, ordered 5_1 helical secondary structure by MM2 calculations, thermal stability and transitions by TGA and DSC, and diffraction patterns by pXRD experiments support the conclusion that the high erythro-diastereoselectivity of the Pin produced by the MAD-based LPs is responsible for its unique material's properties such as insolubility in common organic solvents as well as enhanced thermal stability, T_g, and crystallinity.

The Pin material with a moderate erythro-ditacticity (57%) produced by the FAB/SKA LP was subjected to optical analysis due to having glassy, transparent character. Employing UV/vis/NIR spectroscopy on a 160 μm prepared thin film sample, we found transmittance values between 85 and 89% in the 400−1000 nm region, with no exhibited transmittance in the ultraviolet region due to absorbance by the pendant group chromophores (Figure 7). We further obtained a reflectance value of 9.6% and calculated a haze value of 11.0% (Figures S19 and S20). This level of transparency is competitive with those of widely used transparent commodity plastics, such as amorphous poly(methyl methacrylate) (T_g = 110 °C, T % = ~90%) and poly(styrene) (T_g = 100 °C, T % = ~90%).[47,48] However, Pin fills the gap between high transparency and thermal stability, with a T_g (286 °C) more than 170 °C higher than that of the commodity transparent plastics. Hence, Pin

https://dx.doi.org/10.1021/acs.macromol.9b02285
Macromolecules 2020, 53, 640−648

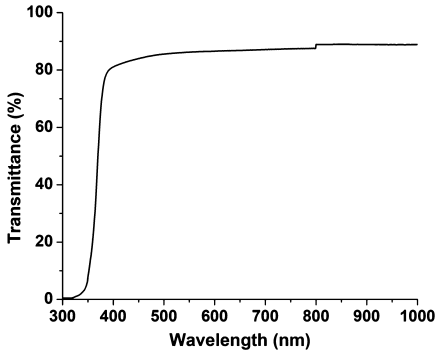

Figure 7. UV/vis/NIR spectrum for the total transmittance of 160 μm Pin thin-film (M_n = 1.72 × 10^5 g mol^{-1}, $Đ$ = 1.23, erythro-ditacticity = 57%, T_g = 286 °C).

could serve rational use in solar cell coatings, in which the transparent material coating the solid-state photovoltaics must be able to withstand elevated temperatures from solar energy as well as filter ultraviolet radiation which damages solar cells.[49] It is worth mentioning that Pin's chain rigidity conduces a very brittle material, rendering the preparation of self-supported films thicker than 160 μm challenging.

Upconversion of Pin to Graphite Oxide. Consistently throughout TGA experiments with Pin, roughly 15% mass remained after the initial decomposition curve as some carbonaceous material stable up to 700 °C. We postulated that the ring-fused phenyl group and the ketone functional handle may promote thermal decomposition of Pin into a useful material that could extend this polymer's end of its first life. We collected decomposed Pin upon treatment in a tube furnace at 360 °C and subjected the material to analysis by pXRD and Raman spectroscopy. pXRD analysis gave 2θ values of 3.4, 24.8, and 42.3°, which were converted to d-spacing multiples of 2.6, 0.36, and 0.21 nm, respectively. Comparing these d-spacing values among indexed material, references gave strong evidence for well-ordered carbon-rich materials (Figure 8a).[50] Through Raman spectroscopy, we observed only three signals matching the vibrational bands for the out-of-phase sp^3 defect region (D-band; 1390 cm^{-1}), the in-phase sp^2 graphitic regions (G-band; 1610 cm^{-1}) for graphite oxide (GO), and a very small 2D-band (Figure 5b).[51] As further supporting evidence for the formation of GO, we subjected the same samples to scanning electron microscopy (SEM) and found signature layering expected of graphitic lamina (Figure 5c,d; 10 μm SEM image shown in Figure S18). Upconversion of Pin was subsequently examined in more detail by varying the Pin erythro content, reaction atmosphere, and pyrolysis temperature (Table S1). Such pyrolysis experiments revealed an inverse correlation between erythro-diastereoselectivity and GO upconversion yield, where atactic Pin yielded 54% GO and the ditactic Pin with the highest erythro-ditactciity yielded only 25% GO. Decomposition of Pin into GO was an exciting find, not only for the versatile applicability of GO in battery applications, energy conversion, and coatings[52] but also because it reveals an upcycling avenue for Pin at the end of its life.

CONCLUSIONS

This contribution details the preparation and storage of unstable monomeric indenone for the effective polymerization using LPs affording, for the first time, high M_w polymers (M_n up to 1.72 × 10^5 g mol^{-1}) with relatively low dispersity values ($Đ$ = 1.13−1.23). These M_w characteristics were measured for the soluble Pin materials with low erythro-diastereoselectivity of 57% produced by the FAB/SKA LP, and it is anticipated the Pin materials with higher erythro-ditacticity of ≥71% produced by MAD-based LPs would be even higher if they can be measured by GPC in common organic solvents. Referring to the predicted propagation TSs, we manipulated the steric bulk of the LA in the LP and realized tunable diastereoselective bias through a chain-end control mechanism to achieve a range of

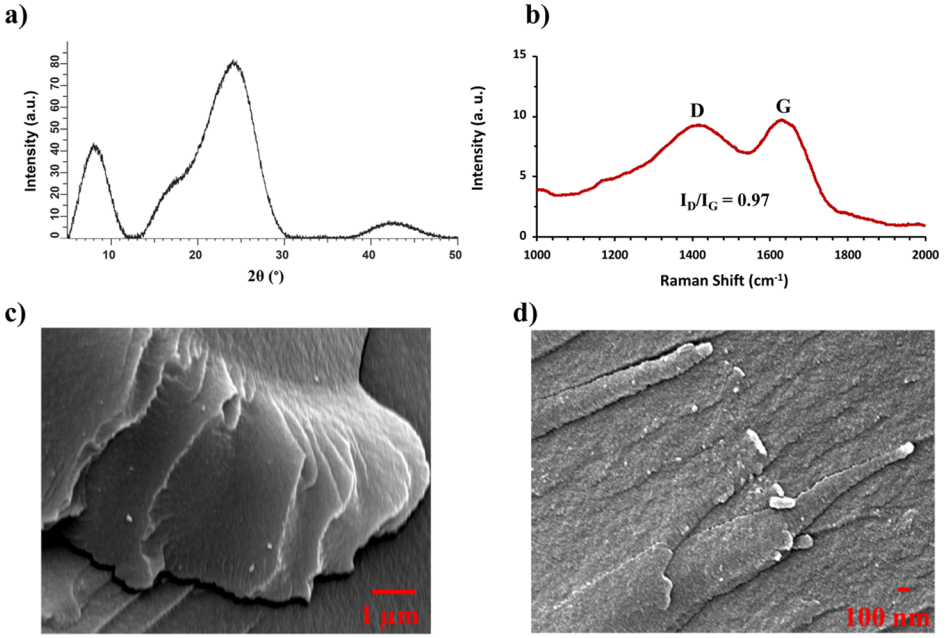

Figure 8. (a) pXRD of pyrolyzed Pin carbonaceous material. (b) Raman spectroscopy of GO obtained from pyrolysis of Pin with labeled D-band, G-band, and the calculated surface defect ratio (I_D/I_G). (c) SEM image of GO at 1 μm scale, highlighting layering characteristic. (d) SEM image of GO at 100 nm scale, consisting of grooved layers.

https://dx.doi.org/10.1021/acs.macromol.9b02285
Macromolecules 2020, 53, 640−648

Pin samples with erythro content between 57 and 75% and significantly enhanced T_g and T_d values of 307 and 356 °C, respectively, relative to the nonselective autopolymerized Pin (T_g = 269 °C and T_d = 329 °C). Collective evidence pointed to a semicrystalline material with an ordered 5_1 helical secondary structure for Pin with high erythro-di(*iso*)tacticity. Analysis of the highly stable (to 700 °C) carbonaceous material generated via pyrolysis of Pin at 360 °C by Raman spectroscopy, pXRD, and SEM provided key evidence for the upconversion of Pin into versatile GO, offering a valuable upcycling avenue to extend this polymer's applicability at the end of its life. Pin also offers valuable applicability as a material with exceptionally high T_g coupled with good transmittance (>85%) and low haziness (11%).

■ ASSOCIATED CONTENT

Supporting Information

The Supporting Information is available free of charge at https://pubs.acs.org/doi/10.1021/acs.macromol.9b02285.

Experimental section, additional ^{1}H and ^{13}C NMR data for monomer storage, stability control experiments, and erythro-diastereoselectivity, NMR assignment discussions, typical polymer spectra, and GO-upconversion experiments (PDF)

■ AUTHOR INFORMATION

Corresponding Author

Eugene Y.-X. Chen − *Colorado State University, Fort Collins, Colorado;* orcid.org/0000-0001-7512-3484; Email: eugene.chen@colostate.edu

Other Authors

Ryan W. Clarke − *Colorado State University, Fort Collins, Colorado*

Michael L. McGraw − *Colorado State University, Fort Collins, Colorado*

Ravikumar R. Gowda − *Colorado State University, Fort Collins, Colorado*

Complete contact information is available at: https://pubs.acs.org/10.1021/acs.macromol.9b02285

Author Contributions

E.Y.-X.C. directed the project. R.W.C. and M.L.M. designed the experiments. R.W.C. synthesized the materials and conducted the polymerizations. R.W.C. and M.L.M. interpreted the data. R.R.G. performed pXRD and SEM experiments. The manuscript was written through contributions of all authors. All authors have given approval to the final version of the manuscript.

Notes

The authors declare no competing financial interest.

■ ACKNOWLEDGMENTS

We gratefully acknowledge the support by the U.S. National Science Foundation (NSF-1904962). We also thank Boulder Scientific Co. for the research gift of $B(C_6F_5)_3$.

■ REFERENCES

(1) Takenaka, Y.; Abe, H. Group-Transfer Polymerization of Various Crotonates Using Organic Acid Catalysts. *Macromolecules* **2019**, *52*, 4052−4058.

(2) McGraw, M. L.; Chen, E. Y.-X. Borane/silane frustrated Lewis pairs for polymerization of β-substituted Michael acceptors. *Tetrahedron* **2019**, *75*, 1475−1480.

(3) McGraw, M.; Chen, E. Y.-X. Catalytic Lewis Pair Polymerization of Renewable Methyl Crotonate to High-Molecular-Weight Polymers. *ACS Catal.* **2018**, *8*, 9877−9887.

(4) Flanagan, J. C. A.; Kang, E. J.; Strong, N. I.; Waymouth, R. M. Catalytic Dimerization of Crotonates. *ACS Catal.* **2015**, *5*, 5328−5332.

(5) Tsuruta, T.; Makimoto, T.; Tanabe, K. Anionic Polymerization of β-substituted Acrylic Esters. *Makromol. Chem.* **1968**, *114*, 182−200.

(6) Bockman, O. C.; Schuerch, C. Anionic Polymerizations via the Michael Reaction. *J. Polym. Sci., Part B: Polym. Lett.* **1963**, *1*, 145−151.

(7) Terao, Y.; Satoh, K.; Kamigaito, M. Controlled Radical Copolymerization of Cinnamic Derivatives as Renewable Vinyl Monomers with Both Acrylic and Styrenic Substituents: Reactivity, Regioselectivity, Properties, and Functions. *Biomacromolecules* **2019**, *20*, 192−203.

(8) Meier, M. A. R.; Metzger, J. O.; Schubert, U. S. Plant Oil Renewable Resources as Green Alternatives in Polymer Science. *Chem. Soc. Rev.* **2007**, *36*, 1788−1802.

(9) Abe, H. Thermal Degradation of Environmentally Degradable Poly(hydroxyalkanoic acid)s. *Macromol. Biosci.* **2006**, *6*, 469−486.

(10) Flanagan, J. C. A.; Myung, J.; Criddle, C. S.; Waymouth, R. M. Poly(hydroxyalkanoate)s from Waste Biomass: A Combined Chemical-Biological Approach. *ChemistrySelect* **2016**, *1*, 2327−2331.

(11) Spekreijse, J.; Le Notre, J.; Sanders, J. P. M.; Scott, E. L. Conversion of Polyhydroxybutyrate (PHB) to Methyl Crotonate for the Production of Biobased Monomers. *J. Appl. Polym. Sci.* **2015**, *132*, 42462−42468.

(12) Hosoi, Y.; Takasu, A.; Matsuoka, S.-I.; Hayashi, M. *N*-Heterocyclic Carbene Initiated Anionic Polymerization of (*E,E*)-Methyl Sorbate and Subsequent Ring-Closing to Cyclic Poly(alkyl sorbate). *J. Am. Chem. Soc.* **2017**, *139*, 15005−15012.

(13) Takasu, A.; Ishii, M.; Inai, Y.; Hirabayashi, T.; Inomata, K. Threo-Disyndiotactic Polymerization of (E,E)-Alkyl Sorbates Assisted by Bulky Organoaluminum Lewis Acid via "Alternating Turning over Polymerization (ATOP)" Mechanism. *Macromolecules* **2003**, *36*, 7055−7064.

(14) Ute, K.; Tarao, T.; Hatada, K. Group Transfer Polymerization of Methyl Crotonate. *Polym. J.* **1997**, *29*, 957−958.

(15) Miller, M. L.; Skogman, J. Polymerization of *tert*-Butyl Crotonate. *J. Polym. Sci., Part A: Gen. Pap.* **1964**, *2*, 4551−4558.

(16) Kitano, T.; Fujimoto, T.; Nagasawa, M. Preparation and Characterization of a Monodisperse, Semiflexible Polymer, Poly(*tert*-butyl crotonate). *Macromolecules* **1974**, *7*, 719−724.

(17) Ute, K.; Tarao, T.; Hongo, S.-y.; Ohnuma, H.; Hatada, K.; Kitayama, T. Preparation of Disyndiotactic Poly(methyl crotonate) by Stereospecific Group Transfer Polymerization. *Polym. J.* **1999**, *31*, 177−183.

(18) Ute, K.; Tarao, T.; Kitayama, T. Enhanced Stereocontrol in Disyndiotactic-specific Group Transfer Polymerization of Methyl Crotonate-Stereochemical Evidence of Group Transfer. *Polym. J.* **2005**, *37*, 578−583.

(19) Tanaka, T.; Matsumoto, A. First Disyndiotactic Polymer from a 1,4-Disubstituted Butadiene by Alternate Molecular Stacking in the Crystalline State. *J. Am. Chem. Soc.* **2002**, *124*, 9676−9677.

(20) Imada, M.; Takenaka, Y.; Hatanaka, H.; Tsuge, T.; Abe, H. Unique Acrylic Resins with Aromatic Side Chains by Homopolymerization of Cinnamic Monomers. *Commun. Chem.* **2019**, *2*, 109.

(21) Schleyer, P. V. R. Introduction: Aromaticity. *Chem. Rev.* **2001**, *101*, 1115−1118.

(22) Breslow, R. Antiaromaticity. *Acc. Chem. Res.* **1973**, *6*, 393−398.

(23) Zhu, J.-B.; Watson, E. M.; Tang, J.; Chen, E. Y.-X. A Synthetic Polymer System with Repeatable Chemical Recyclability. *Science* **2018**, *360*, 398−403.

(24) Kamber, N. E.; Jeong, W.; Waymouth, R. M.; Pratt, R. C.; Lohmeijer, B. G. G.; Hedrick, J. L. Organocatalytic Ring-Opening Polymerization. *Chem. Rev.* **2007**, *107*, 5813−5840.
(25) Hong, M.; Chen, E. Y.-X. Completely recyclable biopolymers with linear and cyclic topologies via ring-opening polymerization of γ-butyrolactone. *Nat. Chem.* **2016**, *8*, 42−49.
(26) Wang, Q.; Zhao, W.; He, J.; Zhang, Y.; Chen, E. Y.-X. Living Ring-Opening Polymerization of Lactones by *N*-Heterocyclic Olefin/Al(C6F5)3 Lewis Pairs: Structures of Intermediates, Kinetics, and Mechanism. *Macromolecules* **2017**, *50*, 123−136.
(27) House, H. O.; Paragamian, V.; Ro, R. S.; Wluka, D. J. The Synthesis of Derivatives of 1-indanone and Indenone. *J. Am. Chem. Soc.* **1960**, *82*, 1452−1457.
(28) Hartless, R. L.; Chandross, E. A. Deep-UV photoresists: Poly(methyl methacrylate-co-indenone). *J. Vac. Sci. Technol.* **1981**, *19*, 1333−1337.
(29) Lin, F.; Wang, M.; Cui, D. Renewable Benzofuran Polymerization Initiated by Lewis Acid Al(C6F5)3 and Mechanism. *Macromolecules* **2017**, *50*, 8449−8455.
(30) Hong, M.; Chen, E. Y.-X. Future Directions for Sustainable Polymers. *Trends Chem.* **2019**, *1*, 148−151.
(31) Pandarus, V.; Gingras, G.; Béland, F.; Ciriminna, R.; Pagliaro, M. Selective Hydrogenation of Alkenes under Ultramild Conditions. *Org. Process Res. Dev.* **2012**, *16*, 1230−1234.
(32) Tran, P. H.; Huynh, V. H.; Hansen, P. E.; Chau, D.-K. N.; Le, T. N. An Efficient and Green Synthesis of 1-Indanone and 1-Tetralone via Intramolecular Friedel-Crafts Acylation Reaction. *Asian J. Org. Chem.* **2015**, *4*, 482−486.
(33) Nguyen, H. T. H.; Qi, P.; Rostagno, M.; Feteha, A.; Miller, S. A. The quest for high glass transition temperature bioplastics. *J. Mater. Chem. A* **2018**, *6*, 9298−9331.
(34) Knaus, M. G. M.; Giuman, M. M.; Pöthig, A.; Rieger, B. End of Frustration: Catalytic Precision Polymerization with Highly Interacting Lewis Pairs. *J. Am. Chem. Soc.* **2016**, *138*, 7776−7781.
(35) Walther, P.; Krauß, A.; Naumann, S. Lewis Pair Polymerization of Epoxides via Zwitterionic Species as a Route to High-Molar-Mass Polyethers. *Angew. Chem., Int. Ed.* **2019**, *58*, 10737−10741.
(36) Ji, H.-Y.; Song, D.-P.; Wang, B.; Pan, L.; Li, Y.-S. Organic Lewis Pairs for Selective Copolymerization of Epoxides with Anhydrides to Access Sequence-Controlled Block Copolymers. *Green Chem.* **2019**, *21*, 6123.
(37) Yang, J.-L.; Cao, X.-H.; Zhang, C.-J.; Wu, H.-L.; Zhang, X.-H. Highly Efficient One-Pot Synthesis of COS-Based Block Copolymers by Using Organic Lewis Pairs. *Molecules* **2018**, *23*, 298−307.
(38) Yang, J.-L.; Wu, H.-L.; Li, Y.; Zhang, X.-H.; Darensbourg, D. J. Perfectly Alternating and Regioselective Copolymerization of Carbonyl Sulfide and Epoxides by Metal-Free Lewis Pairs. *Angew. Chem., Int. Ed.* **2017**, *56*, 5774−5779.
(39) Hong, M.; Chen, J.; Chen, E. Y.-X. Polymerization of Polar Monomers Mediated by Main-Group Lewis Acid-Base Pairs. *Chem. Rev.* **2018**, *118*, 10551−10616.
(40) Wang, Q.; Zhao, W.; Zhang, S.; He, J.; Zhang, Y.; Chen, E. Y.-X. Living Polymerization of Conjugated Polar Alkenes Catalyzed by *N*-Heterocyclic Olefin-Based Frustrated Lewis Pairs. *ACS Catal.* **2018**, *8*, 3571−3578.
(41) Zhang, P.; Zhou, H.; Lu, X.-B. Living and Chemoselective (Co)polymerization of Polar Divinyl Monomers Mediated by Bulky Lewis Pairs. *Macromolecules* **2019**, *52*, 4520−4525.
(42) Zhang, Y.; Miyake, G. M.; John, M. G.; Falivene, L.; Caporaso, L.; Cavallo, L.; Chen, E. Y.-X. Lewis Pair Polymerization by Classical and Frustrated Lewis Pairs: Acid, Base and Monomer Scope and Polymerization Mechanism. *Dalton Trans.* **2012**, *41*, 9119−9134.
(43) Zhang, Y.; Miyake, G. M.; Chen, E. Y.-X. Alane-Based Classical and Frustrated Lewis Pairs in Polymer Synthesis: Rapid polymerization of MMA and Naturally Renewable Methylene Butyrolactones into High-Molecular-Weight Polymers. *Angew. Chem., Int. Ed.* **2010**, *49*, 10158−10162.
(44) Webster, O. W. Living Polymerization Methods. *Science* **1991**, *251*, 887−893.
(45) Webster, O. W.; Hertler, W. R.; Sogah, D. Y.; Farnham, W. B.; RajanBabu, T. V. Group-Transfer Polymerization. 1. A New Concept for Addition Polymerization with Organosilicon Initiators. *J. Am. Chem. Soc.* **1983**, *105*, 5706−5708.
(46) Hu, L.; He, J.; Zhang, Y.; Chen, E. Y.-X. Living Group Transfer Polymerization of Renewable α-Methylene-γ-butyrolactones Using Al(C6F5)3 Catalyst. *Macromolecules* **2018**, *51*, 1296−1307.
(47) Stojanović, D. B.; Brajović, L.; Orlović, A.; Dramlić, D.; Radmilović, V.; Uskoković, P. S.; Aleksić, R. Transparent PMMA/silica Nanocomposites Containing Silica Nanoparticles Coating Under Supercritical Conditions. *Prog. Org. Coat.* **2013**, *76*, 626−631.
(48) Prado, A. d.; Briz, N.; Navarro, R.; Pérez, M.; Gallardo, A.; Reinecke, H. Transparent Polystyrene Substrates with Controllable Surface Chlorosulfonation: Stable, Versatile, and Water-Compatible Precursors for Functionalization. *Macromolecules* **2012**, *45*, 2468−2653.
(49) Malinauskas, T.; Tomkute-Luksiene, D.; Sens, R.; Daskeviciene, M.; Send, R.; Wonneberger, H.; Jankauskas, V.; Bruder, V. Enhancing Thermal Stability and Lifetime of Solid-State Dye-Sensitized Solar Cells via Molecular Engineering of the Hole-Transporting Material Spiro-OMeTAD. *ACS Appl. Mater. Interfaces* **2015**, *7*, 11107−11116.
(50) Skákalová, V.; Kotrusz, P.; Jergel, M.; Susi, T.; Mittelberger, A.; Vretenár, V.; Šiffalovič, P.; Kotakoski, J.; Meyer, J. C.; Hulman, M. Chemical Oxidation of Graphite: Evolution of the Structure and Properties. *J. Phys. Chem. C* **2018**, *122*, 929−935.
(51) Kudin, K. N.; Ozbas, B.; Schniepp, H. C.; Prud'homme, R. K.; Aksay, I. A.; Car, R. Raman Spectra of Graphite Oxide and Functionalized Graphene Sheets. *Nano Lett.* **2008**, *8*, 36−41.
(52) Georgakilas, V.; Tiwari, J. N.; Kemp, K. C.; Perman, J. A.; Bourlinos, A. B.; Kim, K. S.; Zboril, R. Noncovalent Functionalization of Graphene and Graphene Oxide for Energy Materials, Biosensing, Catalytic, and Biomedical Applications. *Chem. Rev.* **2016**, *116*, 5464−5519.

https://dx.doi.org/10.1021/acs.macromol.9b02285
Macromolecules 2020, 53, 640−648